# Magnetic billiards on a torus with a uniform field in a disk

Albert Šilvans, s3400166

June 1, 2023

# Contents

# List of Figures

# List of Tables

# 1   Introduction

Our main point of interest is the long term dynamics of a particle in the presence of a magnetic field, specifically, we consider the case of a magnetic billiard. Similar work has been done in [KS17], where the focus was scattering for finitely many *bumps*, and [Gas21] where many non-trivial periodic orbits were found for "inverted" bumps, that is, the magnetic field only vanished on the bumps. We follow in the same vein but consider infinitely many bumps in a lattice, and describe the dynamics using various methods.

## 1.1   The electromagnetic field Hamiltonian

Classically, the trajectory of a particle in $\mathbb{R}^3$ in the presence of a magnetic field is described by the solutions of the Hamiltonian:

$$H(q,p) = \frac{1}{2m} \left\| p - \frac{e}{c} A(q) \right\|^2 + U(q)$$

where $q = (q_1, q_2, q_3)$ and $p = (p_1, p_2, p_3)$ are the position and momentum, $m, e, c > 0$ are physical parameters, $U : \mathbb{R}^3 \to \mathbb{R}$ is a potential function, and $A : \mathbb{R}^3 \to \mathbb{R}^3$ is a magnetic vector field. For our purposes, we can absorb the physical parameters into the momentum variable and the vector field, effectively, we set $m = e = c = 1$, and we focus on the case $U(q) = 0$ for simplicity. Hence, we study solutions of

$$H(q,p) = \frac{1}{2} \left\| p - A(q) \right\|^2, \tag{1}$$

where $A$ is still to be prescribed. The equations of motion are given by the system:

$$\dot{q}_i = \frac{\partial H(q,p)}{\partial p_i} = p_i - A_i(q) \tag{2a}$$

$$\dot{p}_i = -\frac{\partial H(q,p)}{\partial q_i} = -\sum_{k=1}^{3} \left( p_i - A_i(q) \right) \frac{\partial A_k}{\partial q_i} \tag{2b}$$

where $A_k(q)$ denotes the $k$-th component of $A$. To further limit the breadth of study, we consider some restrictions on $A$. First, we consider only motion in the $(q_1, q_2)$-plane, so only trajectories that have initial condition $q = (q_1, q_2, 0)$ and $p = (p_1, p_2, 0)$, and that satisfy $q_3(t) = p_3(t) = 0$ for all $t \geq 0$. For this to be satisfied, we need that $\dot{q}_3 = p_3 - A_3(q) = 0$, which also implies that $A_3(q) = 0$ for all $t \geq 0$. We also need $\dot{p}_3 = 0$, which means that

$$\left( p_1 - A_1(q) \right) \frac{\partial A_1}{\partial q_3} + \left( p_2 - A_2(q) \right) \frac{\partial A_2}{\partial q_3} = 0.$$

This is a first order differential equation in 2 unknown functions, which is not sufficient to determine a unique solution. An example of a family that satisfies the above:

$$A(q_1, q_2) = (A_1(q_1, q_2), A_2(q_1, q_2), 0).$$

The second criteria we want: $A$ is 1-periodic in $q_1$ and $q_2$, so

$$A(q_1 + 1, q_2 + 1, q_3) = A(q_1, q_2, q_3)$$

In particular, we will later use the vector field $A(q) = (-\varepsilon(q_2 \bmod 1), 0, 0)\mathbb{1}_S$ where $\varepsilon > 0$ and $\mathbb{1}_S$ is the indicator function on $S \subseteq \mathbb{R}^3$ which is a union of cylinders:

$$S = \bigcup_{n,m \in \mathbb{Z}} \left\{ q \in \mathbb{R}^3 : \left(q_1 - n - \frac{1}{2}\right)^2 + \left(q_2 - m - \frac{1}{2}\right)^2 \leq R^2 \right\},$$

where $R \in (0, 1/2)$. Writing out the final form of the Hamiltonian we consider:

$$H(q, p) = \frac{1}{2}\left(p_1^2 + p_2^2\right) + \varepsilon q_2 \left(p_1 + \frac{\varepsilon q_2}{2}\right) \mathbb{1}_S = H_0(q, p) + \varepsilon H_1(q, p, \varepsilon) \tag{3}$$

where we ignore $q_3$ completely. We define $H_0$ and $H_1$ for later use, $H_0$ denotes the unperturbed Hamiltonian and $H_1$ the perturbation.

We immediately notice that (3) is discontinuous along the boundary $\partial S$ of $S$, and this becomes an issue when considering trajectories that pass $\partial S$ tangentially. For some values of $\varepsilon > 0$ we will find that the solution to (3) can be non-unique. We argue however that the dynamics of these solutions is not important, since $\partial S$ is a set of measure zero. Throughout the paper though we assume that if a trajectory does pass $\partial S$ tangentially, then it does not enter $S$.

We also notice that we can express (3) as a Hamiltonian on the torus $\mathbb{T}^2 = \mathbb{R}^2 \backslash \mathbb{Z}^2$ via the usual quotient map which will be convenient for some proofs later. To fully comprehend the dynamics of (3) both in $\mathbb{R}^2$ and $\mathbb{T}^2$ we first discuss the dynamics of each piece separately. That is, we refresh our memory on linear motion in the plane, rotations in a torus, and motion in a uniform magnetic field in the plane.

## 1.2 Linear motion and rotations on the torus

Here we discuss solutions of the Hamiltonian $H : \mathbb{R}^2 \to \mathbb{R}^2$ with $H(q, p) = \|p\|^2/2$ in the plane and in the torus. The equations of motion can be computed readily from the Hamiltonian system, they are:

$$V_1(t) = (q_1(t), q_2(t)), \qquad q_1(t) = p_1 t + q_1(0), \qquad q_2(t) = p_2 t + q_2(0) \tag{4}$$

where $p_1, p_2 \in \mathbb{R}$ are constants. We understand this motion well, it is just straight lines in the plane.

The situation becomes more interesting when we consider the induced motion on the quotient space $\mathbb{T}^2 = \mathbb{R}^2 \backslash \mathbb{Z}^2$ via the quotient $P : \mathbb{R}^2 \to \mathbb{T}^2$ with $P(q_1, q_2) = (q_1 \bmod 1, q_2 \bmod 1) = [q_1, q_2]$, where the bracket indicates the equivalence class of the point $(q_1, q_2)$. The equations become:

$$\hat{V}_1(t) = P \circ V_1(t) = [q_1(t), q_2(t)] = t[p_1, p_2] + [q_1(0), q_2(0)], \tag{5}$$

so the trajectory that was a line in the plane now wraps around the torus. It is now important to understand how the ratio of $p_1$ to $p_2$ influences the dynamics.

**Definition 1.** Let $p_1, p_2 \in \mathbb{R}$, we say $p_1, p_2$ are *rationally dependent* if there exist $n, m \in \mathbb{Z}$ such that $p_1 n + p_2 m = 0$.

Two numbers are then called *rationally independent* if there does not exist a pair of integers satisfying the equation. This definition helps us formulate the following well-known result.

**Proposition 1.** Consider the trajectory $\hat{V}_1$ of (5) in the torus.

1. If $p_1$ and $p_2$ are rationally dependent, then $\hat{V}_1$ is a periodic solution, and its orbit $\hat{V}_1([0, \infty))$ is a closed curve on the torus,

2. If $p_1$ and $p_2$ are rationally independent, then $\hat{V}_1([0, \infty))$ is dense in the torus.

Another result that can be mentioned here but will not be important in our discussion is that due to Proposition 1 the set of periodic orbits is dense in phase space.

## 1.3   Uniform magnetic vector field in the plane

We focus now on (1) and take $A(q) = (-\varepsilon q_2, 0, 0)$ and $\varepsilon > 0$ as used for (3), except, we do not include the indicator $\mathbb{1}_S$. This gives the Hamiltonian for the motion of a particle in the $(q_1, q_2)$-plane in the presence of a vector field in the plane.

$$H(q, p) = \frac{1}{2}(p_1 + \varepsilon q_2)^2 + \frac{1}{2}p_2^2, \tag{6}$$

From $H$, we find Hamilton's equations:

$$\frac{dq_1}{dt} = 2(p_1 + \varepsilon q_2) \qquad\qquad \frac{dq_2}{dt} = 2p_2$$
$$\frac{dp_1}{dt} = 0 \qquad\qquad \frac{dp_2}{dt} = -2\varepsilon(p_1 + \varepsilon q_2).$$

And we can find the equations of motion: $X_2(t) = (q_1(t), q_2(t))$ with

$$q_1(t) = \alpha_1 - R\cos(\varepsilon t + \varphi), \qquad q_2(t) = \alpha_2 + R\sin(\varepsilon t + \varphi)$$

where $\alpha_1, \alpha_2, R, \varphi$ are integration constants. These can be computed explicitly:

$$\alpha_1 = q_1(0) + \frac{p_2(0)}{\varepsilon} \qquad\qquad R = \frac{1}{\varepsilon}\|X_2'(t)\|$$

$$\alpha_2 = q_2(0) - \frac{p_1(0)}{\varepsilon} \qquad\qquad \varphi = \arctan 2\left(p_1(0), p_2(0)\right)$$

where arctan2 behaves like arctan with the added benefit that it correctly determines the quadrant of the angle. From the equations of motion, we see that the orbits are circles which we call *Larmor* circles. The *Larmor* radii $R$ and centers $(\alpha_1, \alpha_2)$ of the circles are determined uniquely by the initial conditions of the particle as we can see above.

## 1.4 interplay of linear motion and magnetic fields

In the previous sections we determined the local behavior of the system (3), that is, outside the magnetic disks the particle travels along straight lines, and in the magnetic disks it travels along arc of circles. Respectively, on a torus, there is winding around the torus, and circular arcs. What is interesting to study now is the interplay of linear motion and deflection. Specifically, considered separately, the two modes of motion are easy to predict, meanwhile, when considered together: a particle leaving a magnetic disk may enter one of the neighboring ones, or given the right conditions, it can evade the disks for a "long" time.

# 2 Weak magnetic field and KAM theory

We begin by recalling Kolmogorov-Arnold-Moser (KAM) theory, state one of the main KAM theorems, and briefly outline the main points of the theory before delving into its application. We refer the reader to [Kna18] and [Ser22] for a more detailed account. We strongly recommend [Pö82] for reference, as it is the version of KAM we use here.

KAM theory is a method for studying perturbations of integrable Hamiltonian systems. Its origins lie in Celestial and Hamiltonian mechanics, where it was used to study the orbits of planets. Hamiltonian mechanics is a strong tool for modeling and studying systems, however it is strongest for conservative systems. Naturally, we find in practice many non-conservative systems, or conservative ones that are too complicated in full, in which case a smaller subsystem is modeled and the rest is viewed as a perturbation. We are interested in the second scenario, we denote by $H^0(q,p)$ an integrable Hamiltonian and by $H^1(q,p,\varepsilon)$ a perturbation.

Focusing on the integrable case, it is known by the Liouville-Arnold theorem that there exist *action-angle* coordinates so that $H^0 := H^0(p)$ can be expressed in terms of the action variable only. The equations of motion in action-angle coordinates are

given by:

$$\dot{q} = \omega, \qquad \dot{p} = 0,$$

where $\omega = \partial_p H^0(p)$ and $\partial_p H^0 : I \to \Omega$ is the so-called *frequency map*. In these action-angle coordinates, the phase space becomes $\mathbb{T}^n \times I$ where $I \subseteq \mathbb{R}^n$ and the dynamics of the system are completely expressed as rotations on the torus. Specifically, phase space is foliated into a family of invariant tori $\mathbb{T}^n \times \{p\}$ for each $p \in I \subseteq \mathbb{R}^n$. We consider only integrable Hamiltonians with a *non-degenerate* frequency map, that is, $\det \partial_p^2 H^0 \neq 0$. Now, KAM deals with Hamiltonians of the form

$$H(q,p) = H^0(p) + \varepsilon H^1(q,p),$$

where $1 \gg \varepsilon > 0$ is considered small, $H^0$ is the integrable part and $H^1$ is the perturbation. We assume that $H$ is $2\pi$-periodic in each component of $q$. What KAM theory ensures is that under the correct conditions, a "large" subset $\Omega_{\gamma,\tau} \subseteq \Omega$, $\gamma, \tau > 0$ of invariant tori of $H^0(p)$ are preserved, though possibly deformed, under the perturbation $H^1$. The set $\Omega_{\gamma,\tau}$ is given by:

$$\Omega_{\gamma,\tau} = \left\{ \omega \in \Omega : |\omega \cdot k| \geq \gamma |k|^{-\tau}, 0 \neq k \in \mathbb{Z}^n \right\}. \qquad (7)$$

<span style="color:red">make sure you understand the Cantor set construction on page 134</span>      (8)

The condition for $\Omega_{\gamma,\tau}$ is called the *small divisor condition*. It can be shown that for $\tau > n - 1$ almost all points in $\mathbb{R}^n$ satisfy such a condition for the right choice of $\gamma$, so we can find such points in $\Omega$ as well. In the statement of the theorem we will see that $\gamma$ cannot be varied and must be fixed, since it comes in as a constant in the bound on the size of the perturbation, so we consider the *Cantor* set

$$\Omega_\gamma = \{\omega \in \Omega : d(\omega, \partial\Omega) \geq \gamma\} \cap \left( \bigcup_{\tau > n-1} \Omega_{\gamma,\tau} \right).$$

We see $\Omega \backslash \bigcup_{\gamma > 0} \Omega_\gamma$ is a set of measure zero, so the measure of $\Omega_\gamma$ becomes large for small $\gamma$ ,justifying the term "large". We can now give the KAM theorem as stated in [Pö82].

**Theorem 1.** Let the integrable Hamiltonian $H^0 : \mathbb{T}^n \times I \to \mathbb{R}$ be real analytic and non-degenerate, such that the frequency map $\partial_p H^0 : I \to \Omega$ is a diffeomorphism and let the perturbed Hamiltonian $H = H^0 + \varepsilon H^1$ be of class $C^{\alpha\lambda + \lambda + \tau}$ with $\lambda > \tau + 1 > n$ and $\alpha > 1$. Then there exists a positive $\gamma$-independent $\delta$ such that for $|\varepsilon| < \gamma^2 \delta$ with $\gamma$ sufficiently small, there exists a diffeomorphism

$$\mathcal{T} : \mathbb{T}^n \times \Omega \to \mathbb{T}^n \times I,$$

which on $\mathbb{T}^n \times \Omega_\gamma$ transforms the equations of motion of $H$ into

$$\dot{\theta} = \omega, \qquad \dot{\omega} = 0.$$

The map $\mathfrak{T}$ is of class $C^\alpha$ for non-integer $\alpha$ and close to the inverse of the frequency map; its Jacobian determinant is uniformly bounded from above and below.

In addition, if $H$ is of class $C^{\beta\lambda+\lambda+\tau}$ with $\alpha \leq \beta \leq \infty$, then one can modify $\mathfrak{T}$ outside $\mathbb{T}^n \times \Omega_\gamma$ so that $\mathfrak{T}$ is of class $C^\beta$ for noninteger $\beta$.

So, for $\omega \in \Omega_\gamma$, we can parametrize an invariant torus via the map $\theta \mapsto \mathfrak{T}(\theta, \omega)$. There are a few theorems in use now that are titled the *KAM theorem,* and they differ mainly whether they discuss analytic or smooth perturbations. It is easier to find sources discussing the analytic versions, since they provide stronger results about the invariant torii. Having said this, we use the $C^r$ version because it is easier to construct smooth approximations of discontinuous functions as opposed to analytically approximating them.

## 2.1  Approximating locally $L^1$ functions for KAM

The Hamiltonian (3) we wish to study is discontinuous, which by itself is not suitable for the KAM theorem. We can, however, smoothly approximate the Hamiltonian by using *mollifiers.* The *standard mollifier* $\varphi : \mathbb{R}^n \to \mathbb{R}$ is the following function:

$$\varphi(x) = \begin{cases} c \exp\left(\frac{1}{|x|^2-1}\right), & |x| < 1 \\ 0, & |x| \geq 1, \end{cases}$$

where $c > 0$ is a scaling factor chosen so that the integral of $\varphi$ over $\mathbb{R}^n$ is 1. Also, $\varphi$ is commonly called a *bump* function, since its support is compact. For $\varepsilon > 0$, let

$$\varphi_\varepsilon(x) = \frac{1}{\varepsilon^n} \varphi\left(\frac{x}{\varepsilon}\right),$$

this function has the following properties:

$$\varphi_\varepsilon \in C_c^\infty(\mathbb{R}^n), \quad \varphi \geq 0, \quad \int_{\mathbb{R}^n} \varphi = 1, \quad \operatorname{supp}(\varphi_\varepsilon) \subset B_\varepsilon(0) = \{x \in \mathbb{R}^n : |x| < \varepsilon\},$$

that is, the function $\varphi_\varepsilon$ is smooth in $\mathbb{R}^n$ with compact support, it is positive, its integral is 1, and the support of $\varphi_\varepsilon$ is fully contained in the unit ball of radius $\varepsilon > 0$ centered at the origin.

Let $f \in L^1_{\text{loc}}(X)$ be a locally integrable function in $X \subseteq \mathbb{R}^n$. The *mollification* of $f$ is defined as the convolution of $f$ with $\varphi_\varepsilon$, that is, $\varphi_\varepsilon * f : X_\varepsilon \to \mathbb{R}$ where $X_\varepsilon = \{x \in X : d(x, \partial X) > \varepsilon\}$. Explicitly,

$$f_\varepsilon(x) = (\varphi_\varepsilon * f)(x) = \int_X \varphi_\varepsilon(x-y)f(y)dy = \int_{B_\varepsilon(0)} \varphi_\varepsilon(y)f(x-y)dy, \quad x \in X_\varepsilon$$

Some properties that the mollification $f_\varepsilon$ has are summarized here:

**Theorem 2.** Let $f \in L^1_{\text{loc}}(X)$. Then the mollification $f_\varepsilon$ has the following properties:

1. $f_\varepsilon \in C^\infty)(X_\varepsilon)$,

2. $f_\varepsilon \to f$ almost everywhere as $\varepsilon \to 0$,

3. if $f$ is continuous on $X$, then $f_\varepsilon \to f$ as $\varepsilon \to 0$ uniformly on compact subsebts of $X$,

4. if $1 \leq p < \infty$ and $f \in L^p_{\text{loc}}(X)$, then $f_\varepsilon \to f$ as $\varepsilon \to 0$ in $L^p_{\text{loc}}(X)$

*Proof.* The proof of this theorem can be found in Appendix C of [Eva98]        ∎

What we gain from Theorem 2 is not only a smooth approximation of our discontinuous Hamiltonian but an approximation that can be made arbitrarily precise almost everywhere. Of course, the points which cannot be approximated accurately are concentrated at the boundary of each disk, where the discontinuities lie. Despite this, it is reasonable to assume that for sufficiently small values of $\varepsilon$, the flow of the equations of motion provided by the mollified Hamiltonian approximate very well the flow of the disconitinuous one.



(a)                                        (b)                                        (c)
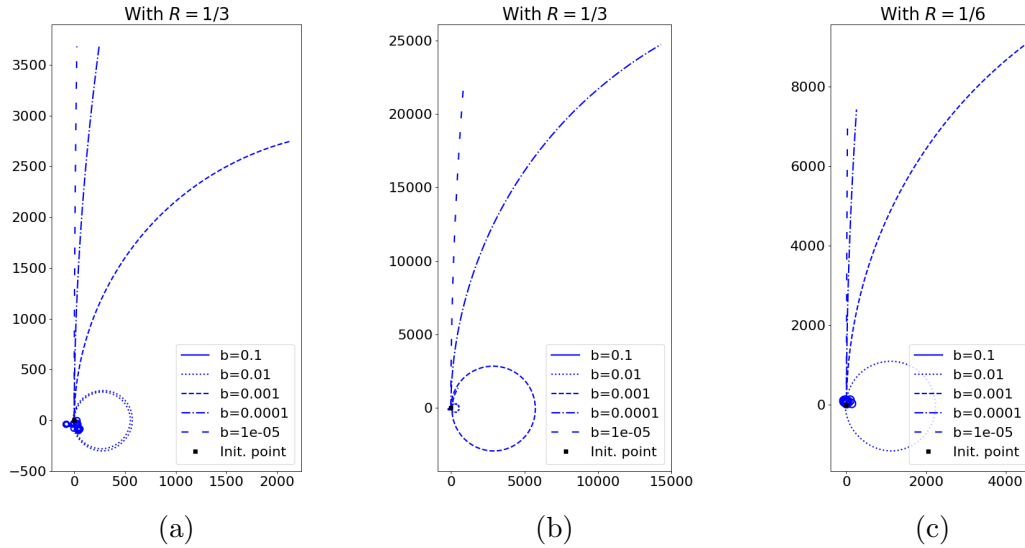
Figure 1: Each plot shows 5 trajectories for varying $b = 10^{-1}, \ldots, 10^{-5}$. In fig. 1a and fig. 1b the init. cond. and params. are the same $X \approx (0.38, 0.81)$ and $V \approx (0, 1)$, and $R = 1/3$, only the duration of the simulation differs. In fig. 1c, $V$ is the same, $X \approx (0.44, 0.65)$ and $R = 1/6$.

In fig. 1 we numerically solve the system and observe some interesting relations. First, we see in each figure the trajectory for $b = 0.1$ appears as a smear near the origin, this is likely because $b$ is large enough for the deflection in each disk to be

significant. For the other values of $b$, we see the trajectories follow a circular arc, and for smaller $b$ the radius of the respective circular arc is larger. In the limit $b \to 0$, the trajectories will straighten out, since the magnetic field vanishes. This motivates the use of KAM, specifically, considering the Hamiltonian $H_0(q, p) = \|p\|^2/2$ and introducing the bumps as a perturbation when $b \approx 0$.

Alternatively, since the trajectories follow circular arcs, this suggests we can consider the motion as a perturbation of a different Hamiltonian. Specifically, we conjecture that we should start with a non-zero magnetic Hamiltonian with vector potential $A = (-\hat{b}q_2, 0, 0)$ in the plane with strength $\hat{b}$ and perturb it to the case with the bumps of strength $b$.

We first reason heuristically to see that this idea is valid. Comparing the trajectories for $b = 0.01$ and $0.001$ in fig. 1a and 1b, we see that the radius of the trajectory is $\approx 250$ and $\approx 2500$, respectively. If we assume this is the value of the Larmor radius $\hat{L}$ in each case, then we see $\hat{L} \propto 1/b$ or $\hat{b} \propto b$. Now, comparing the trajectories for $b = 0.01$ in fig. 1a and 1c, we see halving the radius $R$ of the magnetic bumps roughly quadruples the radius $\hat{L}$ from 250 to 1000, that is, $\hat{L} \propto 1/R^2$, and the strength then relates as $\hat{b} \propto R^2 b$. The task then is to determine $C \in \mathbb{R}$ such that $\hat{b} = CR^2 b$.

We can reason another way. W.l.o.g. consider $[0,1]^2$, we would like the uniform field with strength $\hat{b}$ to have the similar deflection of trajectories as the field with strength $b$ in the disk with radius $R$. How much a trajectory is deflected depends on the flux of the field, so if we equate the fluxes $\Phi_B = \Phi_{\hat{B}}$, we can compute the required strength $\hat{b}$ for $\hat{B}$. Recall, that the magnetic flux is given by:

$$\Phi_B = \iint_S \mathbf{B} \cdot dA = \iint_S \nabla \times \mathbf{A} \cdot dA,$$

so it is the integral of the vector field $\mathbf{B}$ through the surface $S$. Computing the flux for a uniform field in $S$, we get

$$\Phi_{\mathbf{B}} = \iint_S \mathbf{B} \cdot dA = \iint_S (0, 0, b) \cdot (0, 0, 1) dA = bA(S),$$

where $A(S)$ denotes the area of the surface. In our case, $\Phi_{\hat{\mathbf{B}}} = \Phi_{\mathbf{B}}$ implies $\hat{b} = \pi R^2 b$, which is about what we expected. We collect and process some data that corroborates this finding in a later section.

## 2.2   Perturbations of linear motion

Recall, that a particle in the plane moves along Larmor circles when in the presence of a uniform magnetic field, with strength $b$, orthogonal to the plane of motion. The Larmor radius $R$ depends inversely with respect to the field strength, $Rb \propto 1$, that is, a weaker the field strength corresponds to a larger Larmor radius. So, as $b \to 0$, we expect $R \to \infty$, which means that locally the trajectory approaches linear motion in

the plane. This intuition is coroborated when considering the Hamiltonian (6) and setting $\varepsilon = 0$. Hence, it is natural to consider the Hamiltonian $H_0(q, p) = \|p\|^2/2$ and study perturbations of it via KAM

We readily see that $H_0$ is real analytic, it is already in action-angle coordinates from which we can deduce it is non-degenerate $\det \partial_p^2 H_0 = 1 \neq 0$, and the frequency map $\partial_p H_0(p) = p$ is a diffeomorphism. Now, recall the Hamiltonian (3) with $A(q) = (-b(q_2 \bmod 1), 0, 0)\mathbb{1}_S$ where $S$ is the set of disks in the plane, and attempt to isolate the perturbation term from the linear motion.

$$
\begin{aligned}
H(q, p) = \frac{1}{2}\|p - A(q)\|^2 &= \frac{1}{2}\left(p_1 + b(q_2 \bmod 1)\mathbb{1}_S\right)^2 + \frac{1}{2}p_2^2 \\
&= \frac{1}{2}\left(p_1^2 + 2p_1 b(q_2 \bmod 1)\mathbb{1}_S + b^2(q_2^2 \bmod 1)\mathbb{1}_S^2\right) + \frac{1}{2}p_2^2 \\
&= \frac{\|p\|^2}{2} + b\frac{(q_2 \bmod 1)}{2}\left(2p_1\mathbb{1}_S + b(q_2 \bmod 1)\mathbb{1}_S^2\right) \\
&= \frac{\|p\|^2}{2} + b\frac{(q_2 \bmod 1)}{2}\left(2p_1 + b(q_2 \bmod 1)\right)\mathbb{1}_S \\
&= H_0(q, p) + bH_1(q, p, b)
\end{aligned}
$$

where we used $\mathbb{1}_S^2 = \mathbb{1}_S$ for indicator functions. We see now explicitly the perturbation $H_1$. As previously discussed, $H_1$ is discontinuous on $\mathbb{R}^2$, and to apply KAM, we need to mollify $H_1$. Hence, consider the standard mollifier $\varphi_\varepsilon(q, p) = \varphi_\varepsilon(x) : \mathbb{R}^2 \to \mathbb{R}$ and let $\hat{H}_1 = \varphi_\varepsilon * H_1$, notice that we do not mollify with respect to the parameter $b$.

Now, $\hat{H} = H_0 + b\hat{H}_1$. Recalling Theorem 1 we need $\hat{H}$ to be at least of class $C^{\alpha\lambda+\lambda+\tau}$ with $\lambda > \tau + 1 > n = 2$ and $\alpha > 1$. Since $\hat{H}$ is smooth, we can choose any $\tau > 1$, and Theorem 1 guarantees for sufficiently small $\gamma > 0$, there exists a $\delta > 0$ such that for field strengths $b$ with $|b| < \gamma^2\delta$ we can preserve the invariant tori with frequencies in $\Omega_\gamma$.

## 2.3 Perturbation of motion in a constant field

From fig. 1 we saw that instead of perturbing a linear Hamiltonian, we can try perturbing a Hamiltonian for a uniform magnetic field in the plane. If $R$ is the radius of the magnetic disks, $b$ the strength of the field, $L$ the Larmor radius for $b$, and likewise for $\hat{L}$ and $\hat{b}$, we proposed a relation $\hat{b} = \pi R^2 b$. To verify this relation, we instead use $\hat{L} = L/(\pi R^2)$, since $L$ and $R$ are parameters to choose and we can approximate $\hat{L}$ from the time series data. Our problem is then to check the order of $\hat{L} - L/(\pi R^2)$ for some choices of $L$ and $R$.

To approximate $\hat{L}$ we use the method of I. Coope which uses a change of coordinates to bring a non-linear least squares problem to the form of a linear problem. The set up and advantages of this method are discussed in [Coo93], and our use of it can be viewed at [??].

To collect data we tried 15 different pairs of parameters $(R, b)$ chosen at random uniformly from the range $(0.05, 0.49) \times (10^{-5}, 10^{-2})$. For each pair $(R, b)$, we chose 20

|   | $R$ | $b$ | $\hat{L}$ (avg. over 20) | $\Delta = \pi\hat{L}R^2 b - 1$ |
|---|---|---|---|---|
| 1 | $2.335 \cdot 10^{-1}$ | $6.708 \cdot 10^{-3}$ | $8.804 \cdot 10^{2}$ | $1.144 \cdot 10^{-2}$ |
| 2 | $3.669 \cdot 10^{-1}$ | $4.179 \cdot 10^{-3}$ | $5.604 \cdot 10^{2}$ | $9.342 \cdot 10^{-3}$ |
| 3 | $5.005 \cdot 10^{-2}$ | $5.591 \cdot 10^{-3}$ | $2.259 \cdot 10^{4}$ | $5.820 \cdot 10^{-3}$ |
| 4 | $1.830 \cdot 10^{-1}$ | $1.412 \cdot 10^{-3}$ | $6.856 \cdot 10^{3}$ | $1.916 \cdot 10^{-2}$ |
| 5 | $1.146 \cdot 10^{-1}$ | $1.989 \cdot 10^{-3}$ | $1.205 \cdot 10^{4}$ | $1.161 \cdot 10^{-2}$ |
| 6 | $9.063 \cdot 10^{-2}$ | $8.009 \cdot 10^{-3}$ | $4.918 \cdot 10^{3}$ | $1.642 \cdot 10^{-2}$ |
| 7 | $1.320 \cdot 10^{-1}$ | $9.683 \cdot 10^{-3}$ | $1.876 \cdot 10^{3}$ | $6.147 \cdot 10^{-3}$ |
| 8 | $2.020 \cdot 10^{-1}$ | $3.141 \cdot 10^{-3}$ | $2.492 \cdot 10^{3}$ | $3.778 \cdot 10^{-3}$ |
| 9 | $2.246 \cdot 10^{-1}$ | $6.926 \cdot 10^{-3}$ | $8.982 \cdot 10^{2}$ | $1.432 \cdot 10^{-2}$ |
| 10 | $2.871 \cdot 10^{-1}$ | $8.765 \cdot 10^{-3}$ | $4.403 \cdot 10^{2}$ | $7.760 \cdot 10^{-4}$ |
| 11 | $2.344 \cdot 10^{-1}$ | $8.947 \cdot 10^{-3}$ | $6.374 \cdot 10^{2}$ | $1.518 \cdot 10^{-2}$ |
| 12 | $3.515 \cdot 10^{-1}$ | $8.596 \cdot 10^{-4}$ | $3.012 \cdot 10^{3}$ | $4.836 \cdot 10^{-3}$ |
| 13 | $1.400 \cdot 10^{-1}$ | $4.002 \cdot 10^{-4}$ | $4.285 \cdot 10^{4}$ | $5.532 \cdot 10^{-2}$ |
| 14 | $4.364 \cdot 10^{-1}$ | $1.707 \cdot 10^{-3}$ | $9.944 \cdot 10^{2}$ | $1.525 \cdot 10^{-2}$ |
| 15 | $6.205 \cdot 10^{-2}$ | $8.783 \cdot 10^{-3}$ | $9.271 \cdot 10^{3}$ | $1.513 \cdot 10^{-2}$ |

Table 1: Given $R$ and $b$, we find the radius of a circle fit to a trajectory starting at a random initial condition. The average radius $\hat{L}$ is computed over 20 samples. The last column checks how well our ansatz fits

initial conditions at random and computed the corresponding trajectories for some finite time. For each trajectory we fit a circle as described above and were left with 20 values for $\hat{L}$. Finally, we took the average over the 20 values of $\hat{L}$ assuming the average best represents the true value of $\hat{L}$. To judge the plausibility of our model we computed $\Delta = \pi\hat{L}R^2 b - 1$.

Overall, the results show that our assumptions are plausible, since $\Delta$ is small. However, comparing individual results, we see some inconsistencies. For example, comparing runs 10 and 11, we see that $R$ and $b$ are comparable in magnitude however their computed $\Delta$ differ in magnitude. The same can be noticed for runs 3 and 15, and even 1 and 2. We do not attribute this to the circle fitting method, when testing the code, the fitting appeared reasonable. Instead this discrepancy is likely due to the random choice of initial conditions for each run. The trajectory of one initial condition could have shorter flights outside the magnetic disks leading to more deflection, and more curving, hence a nicer circle, and some trajectories could have longer flights which would produce a curve that is more of an ellipse.

Conclusion...

# 3   Stability analysis via Poincaré sections

In the last two sections we discussed linear motion in the plane and motion with a uniform vector field in the plane. Now, we understand the motion of (3): within $S$ the motion follows an arc of a Larmor circle, and outside $S$ the motion is linear. We notice that we can describe the motion solely using analytic geometry, that is, the dynamics is determined by intersections of lines with circles or circles with circles, with the exception of trajectories that are tangent to $\partial S$ which we discussed before and have since ignored.

We present now, and prove later, that the continuous time motion of (3) can be characterized discretely, that is, we can pick a Poincaré section and a Poincaré map.

We notice that the dynamics of the system can be broken down into two modes: the first linear motion outside the magnetic disk, and the second being deflection in the disk. If a trajectory with initial condition on the boundary of the disk always returns to the boundary of the disk we can compress the system from continuous time to discrete time via a Poincaré map. We would then like to prove that the boundary of the magnetic region with the set of outward pointing velocities, that is,

$$S = \bigcup_{\theta \in [0, 2\pi]} \{\theta\} \times \left[\theta - \frac{\pi}{2}, \theta + \frac{\pi}{2}\right] \tag{9}$$

is a Poincaré section. To prove this we need to recall rotations on a torus. If the angle of rotation is irrational, then the trajectory fills the torus densely, if the angle is rational, then the trajectory is periodic and a closed loop. To complete the statement, we need the Poincaré map $P$ itself, here we state the form of the map but we are too lazy for now.

We define the map $P$ already assuming that the trajectory returns for sure. We prove that it does now:

**Proposition 2.** The set $S$ as in (9) is a Poincaré section for the system, and the map $P : U \to P(U)$ is a Poincaré map.

*Proof.* We need to prove that a trajectory of the system with initial condition in $S$ returns to $S$. Notice that if a trajectory enters the disk transversally, it will exit the disk transversally as well. This means if we can show that if all initial conditions in $S$ have a time $t$ at which their trajectory is on the disk and is pointing inward, then we are done.

Let $(x, v) \in S$, and consider the trajectory of the system evolving with this initial condition. If $v$ is a rational angle, then the trajectory corresponding to rotations on the torus is periodic, and there exists a time $t > 0$ at which we return to the same point $x$. Since $(x, v)$ is transversal to the disk, this means there exists a time $t_1 < t$ when the trajectory is on the boundary of the disk and has velocity pointing inward the disk.

13

If $v$ is an irrational angle, then the trajectory corresponding to rotations on the torus is dense in the torus. Let $U$ be a neighborhood of $x$ in the boundary of the disk, such that all $U \times \{v\}$ are transversal to the disk. This is possible, since $(x, v)$ itself is transversal. Pick $y \in U$, then for some $t > 0$ the trajectory of the rotation is at $y$ with velocity $v$, that is the trajectory is transversal. Following the same reasoning as the previous case, there is a time $t_1 < t$ at which the trajectory must enter the disk.

We have shown that the trajectory of the rotation returns to the disk and points inward in finite time, and at least once. For the Poincaré map we then take the first time the trajectory returns to the disk. ∎

Using the Poincaré map we can study the stability of periodic trajectories of the system. The computations become unwieldy on paper, so we use a computer. The code for this can be found at insert code reference [??]

The code written in `Python` utilizes the symbolic algebra system `Sympy` to define functions, compute derivatives, compose functions, and compute eigenvalues of a Jacobian symbolically. That way we avoid a considerable amount of computation by hand but still retain a high degree of precision when computing numerical values. For long enough periodic orbits, the computation time using symbolic algebra becomes unreasonable, so we require a different way to analyse stability. A common alternative is to compute Lyapunov exponents of the original system or of the Poincaré map. However, these approaches are prone to numerical instability and require significant preparation beforehand. We would like to analyze stability from the trajectory directly, and we attempt this via symbolic dynamics in the next section.

With $B_r(q) \subset \mathbb{R}^2$ denote the closed ball of radius $r > 0$ centered at $q \in \mathbb{R}^2$. Pick $S = \cup_{N \in \mathbb{Z}^2} B_{1/3}(N - 1/2)$, that is, $S$ is the union of closed balls of radius $1/3$ centered at points of the form $(n - 1/2, m - 1/2)$ for $n, m \in \mathbb{Z}$.

The choice of radius $r = 1/3$ is arbitrary, we fix it for convenience. Furthermore, we notice the speed of the particle is constant, since $\|X'(0)\| = Rb$, so again for simplicity we fix $\|X'(0)\| = 1$. This also fixes the Larmor radius $R = 1/b$. A different choice of $r \in (0, 1/2)$ and $\|X'(0)\| \in (0, \infty)$ clearly gives rise to different dynamics, however we make the assumption that the dynamics will not differ *qualitatively*, i.e., in any case we expect to find periodic orbits, chaotic behavior, and the methods we use for studying these are still valid.

Hence, we study the influence of varying the parameter $b > 0$ on the above defined system. What we see is four ranges of behavior:

1. For values $b \approx 0$ we can approximate the dynamics as a perturbation of a system with no magnetic field at all,

2. For a range of "small" values of $b$, the dynamics are similar to that of a uniform field in $\mathbb{R}^2$,

3. there is an intermediate range where both stable and unstable periodic dynamics occur

4. there exists a value $b_t$, such that all values $b > b_t$ give rise to unstable dynamics.

We can use this to already find some simple periodic orbits. We describe one such orbit now.

Let $\delta \in (0, 1/3)$ and consider the initial condition $(x, p) = (0, 1/2 + delta, 1, 0)$, the trajectory can be seen in fig. 2a. We can compute that for the choice $b = 1/\delta$, the trajectory will be a periodic orbit.

Already, we see that periodic orbits exist for arbitrarily large $b$. It can be shown using Poincaré sections that this family of periodic orbits is unstable.

Another family of periodic orbits are given for $\delta \in (-1/\sqrt{18}, 1/3)$, where the initial condition is $(x, p) = (0, 1/2 + \delta, 1, 0)$ and $b = 1/(\delta + \sqrt{1/9 - \delta^2})$

Another family of periodic orbits are given for $\delta \in (1/\sqrt{18}, 1/3)$, where the initial condition is $(x, p) = (0, 1/2 + \delta, 1, 0)$ and $b = 1/(\delta - \sqrt{1/9 - \delta^2})$

Lastly, we have a more complicated periodic orbit that forms an octagon for

# 4   Lempel-Ziv complexity and symbolic dynamics

In the previous section, we attempted to assess the stability properties of the system by means of a Poincaré map. We found that there are families of both stable and unstable periodic orbits, and we also proved this with symbolic algebra. Now, we approach the question from the perspective of symbolic dynamics, and use the Lempel-Ziv compression algorithm to measure the complexity of trajectories.

The Lempel-Ziv complexity is a measure of complexity suited for finite length sequences with finite alphabet. This means we need to decide how to extract some symbolic dynamics from the continuous time trajectories of the system. We will describe this after we define the Lempel-Ziv compression algorithm.

As the authors, Abraham Lempel and Jacob Ziv, state in their paper [LZ76] their complexity is not a measure of randomness, which they believe cannot exist, instead they proposed to evaluate "the complexity of a finite sequence from the point of view of a simple self delimiting learning machine". That is, a machine that scans the sequence by entry and records the number of "new" data accumulated, which in this case is unique substrings.

To explain the algorithm, we use a series of examples, as in the paper [KS87]. We are not interested in the technicalities of the original paper by Lempel and Ziv, so we only cite results when needed.
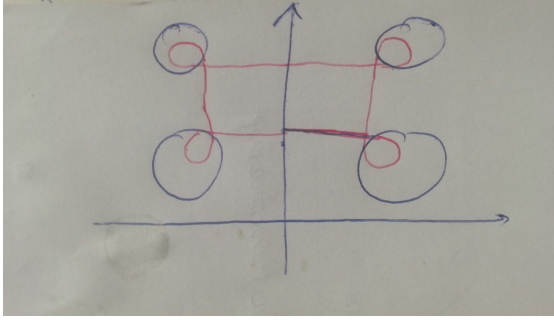
Consider a sequence $s = s_1 s_2 \ldots s_n$ of length $n \in \mathbb{N}$, where we see that $s_i$ is the entry at index $i$ in the sequence, the algorithm decides what is the smallest number of "words" in the sequence necessary for reconstruction. Suppose we have reconstructed $s$ up to the index $k < n$ and the word counter is $c$, that is, we have
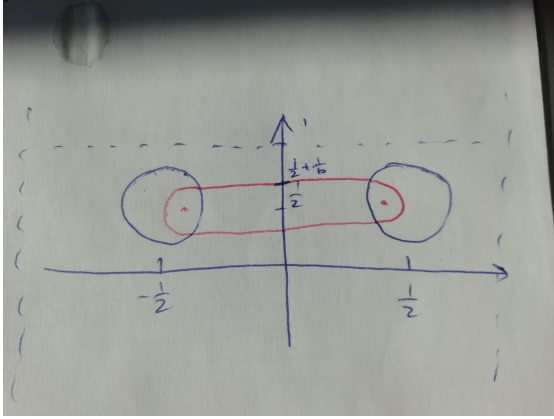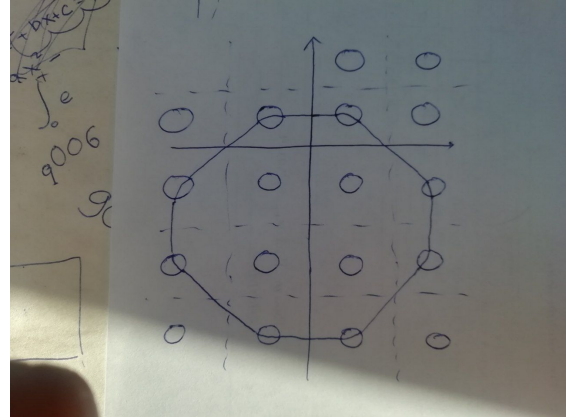
(a) $(x, p) = (0, 1/2 + \delta, 1, 0)$ and $b = 1/\delta$ where $\delta \in (0, 1/3)$.
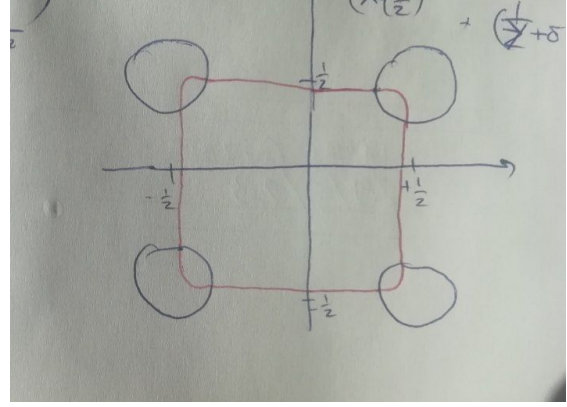


(b) $(x, p) = (0, 1/2 + \delta, 1, 0)$ and $b = 1/(\delta + \sqrt{1/9 - \delta^2})$ where $\delta \in (-1/\sqrt{18}, 1/3)$.



(c) $(x, p) = (0, 1/2 + \delta, 1, 0)$ and $b = 1/(\delta - \sqrt{1/9 - \delta^2})$ where $\delta \in (1/\sqrt{18}), 1/3$.



(d) $(x, p) = (0, 1/2 + \delta, 1, 0)$ and $b = 1/(\delta - \sqrt{1/9 - \delta^2})$ where $\delta \in (1/\sqrt{18}), 1/3$.

Figure 2: Some families of periodic orbits with initial condition $(x, p)$ and magnetic field strength $b$, parametrized by $\delta > 0$.

$s_1 \ldots s_k$. For the next iteration, the algorithm decides what is the largest $k < \ell \leq n$ such that the subsequence $s_{k+1} \ldots s_\ell$ appears at some index in $s_1 \ldots s_{\ell-1}$. Once this $\ell$ is found, the word counter is increased to $c + 1$, if $\ell = n$, then the algorithm terminates, otherwise the process is repeated with $s_1 \ldots s_{\ell+1}$. If $\ell + 1 = n$, then we are done as well. Consider the example sequence 01011010001101110010, we indicate below each step of the algorithm. The $\cdot$ is used as a delimiter between words, and the top line indicates the longest subsequence we can find at each iteration, and the bottom line shows where they can be found.

16

$$\overline{0}1011010001101110010 \xrightarrow{(1)} 0 \cdot \overline{1}011010001101110010$$

$$\xrightarrow{(2)} \underline{0 \cdot 1} \cdot \overline{01}1010001101110010$$

$$\xrightarrow{(3)} \underline{0 \cdot 1 \cdot 011} \cdot \overline{010}001101110010$$

$$\xrightarrow{(4)} 0 \cdot 1 \cdot \underline{011 \cdot 01}00 \cdot \overline{01101}110010$$

$$\xrightarrow{(5)} 0 \cdot 1 \cdot 011 \cdot 0\underline{100} \cdot 011011 \cdot \overline{100}10$$

$$\xrightarrow{(5)} \underline{0} \cdot 1 \cdot 011 \cdot 0100 \cdot 011011 \cdot 1001 \cdot \overline{0}$$

$$\xrightarrow{(6)} 0 \cdot 1 \cdot 011 \cdot 0100 \cdot 011011 \cdot 1001 \cdot 0$$

At the start, we scan from the left, and notice we have never encountered a 0, so for step (1) we add 0 on its own. Next, we encounter 1 for the first time, and add it in step (2). Next, we see that we have encountered 01, so we add 011. Notice, how we ignore the delimiter between words. We indicate the rest of the steps without commentary. Once the algorithm terminates, we see that the number of words is 7, so the complexity of this sequence is 7. The complexity is not normalized to $[0, 1]$ generally, however it is convenient to consider the *compression ratio*, which in this case is $7/20 = 0.35$, that is, we compressed a sequence of 20 symbols to 7 bits of information. We note that the compression ratio is mostly useful for comparing the compression of sequences of the same length. If we take the sequence in the above example and add a 1 at the end, then the complexity will stay 7, which then means the compression ratio is now $7/21 = 0.33\ldots$, which is smaller than before, and that does not fit well with the intuition that complexity is non-decreasing with respect to the length of a sequence.

Now, that we have an idea how the Lempel-Ziv (LZ) complexity is computed, we can discuss how LZ capture the regularity (or lack of it) in symbolic dynamics.

# 5   Levy Flights

# 6   Conclusion

## 6.1   Further questions

|                                   | $b \ll 1$    | $b \approx 1$                         | $b \gg 1$                                       |
| --------------------------------- | ------------ | ------------------------------------- | ----------------------------------------------- |
| Uniform perturbation in a disk    | Circle Maps  | test cases (difficult in general)     | Perturbation of Sinai Billiards (maybe)         |
| Arbitrary perturbations           | Usual KAM    | use paper by Donnay-Liverani          | Hard?                                           |

Table 2: What it is that we want to do

# References

[Coo93] I. D. Coope. Circle fitting by linear and nonlinear least squares. *Journal of Optimization Theory and Applications*, 76:381–388, Feb 1993. `https://doi.org/10.1007/BF00939613`.

[Eva98] Lawrence C. Evans. *Partial Differential Equations*. American Mathematics Society, 1998. Providence, RI.

[Gas21] Sean Gasiorek. On the dynamics of inverse magnetic billiards. *Nonlinearity*, 34(3):1503–1524, mar 2021. `https://doi.org/10.1088%2F1361-6544%2Fabe2f1`.

[Kna18] Andreas Knauf. *Mathematical Physics: Classical Mechanics*. Springer Berlin, Heidelberg, mar 2018. `https://doi.org/10.1007/978-3-662-55774-7`.

[KS87] Kaspar and Schuster. Easily calculable measure for the complexity of spatiotemporal patterns. *Physical review. A, General physics*, 36 2:842–848, 1987.

[KS17] Andreas Knauf and Marcello Seri. Symbolic dynamics of magnetic bumps. *Regular and Chaotic Dynamics*, 22(4):448–454, jul 2017. `https://doi.org/10.1134%2Fs1560354717040074`.

[LZ76] A. Lempel and J. Ziv. On the complexity of finite sequences. *IEEE Transactions on Information Theory*, 22(1):75–81, January 1976.

[Pö82] Jürgen Pöschel. Integrability of hamiltonian systems on cantor sets. *Communications on Pure and Applied Mathematics*, 35(5):653–696, 1982. `https://onlinelibrary.wiley.com/doi/abs/10.1002/cpa.3160350504`.

[Ser22]   Marcello Seri. *Hamiltonian Mechanics.* AMS Open Math Notes, mar 2022.   `https://www.ams.org/open-math-notes/omn-view-listing?listingId=110861`.